Gravitational Potential Energy Balance for the Thermal Circulation in a Model Ocean

RUI XIN HUANG AND XINGZE JIN

Department of Physical Oceanography, Woods Hole Oceanographic Institution, Woods Hole, Massachusetts

(Manuscript received 6 November 2003, in final form 7 October 2005)

ABSTRACT

The gravitational potential energy balance of the thermal circulation in a simple rectangular model basin is diagnosed from numerical experiments based on a mass-conserving oceanic general circulation model. The vertical mixing coefficient is assumed to be a given constant. The model ocean is heated/cooled from the upper surface or bottom, and the equation of state is linear or nonlinear. Although the circulation patterns obtained from these cases look rather similar, the energetics of the circulation may be very different. For cases of differential heating from the bottom with a nonlinear equation of state, the circulation is driven by mechanical energy generated by heating from the bottom. On the other hand, circulation for three other cases is driven by external mechanical energy, which is implicitly provided by tidal dissipation and wind stress. The major balance of gravitational energy in this model ocean is between the source of energy due to vertical mixing and the conversion from kinetic energy at low latitudes and the sink of energy due to convection adjustment and conversion to kinetic energy at high latitudes.

1. Introduction

Thermohaline circulation plays a vital role in climate. However, the exact meaning of thermohaline circulation remains ill-defined (Wunsch 2002). A commonly accepted theory is that the meridional buoyancy difference controls the circulation, and this is the connotation associated with the thermohaline circulation.

This commonly held theory is now being challenged because it appears that the thermohaline circulation is not driven by surface thermohaline forcing; instead, it is driven by mechanical energy sources, such as wind stress and tides. A new paradigm is emerging; the meridional circulation in the ocean is controlled by the external mechanical energy from wind stress and tidal dissipation (e.g., Munk and Wunsch 1998; Huang 1999, 2004; Wunsch and Ferrari 2004). As a working definition, the thermohaline circulation discussed in this study is defined as follows: the meridional overturning flow in the ocean is driven by mechanical energy (from tides and wind stress), which transports heat, freshwater, and other properties. In addition, the surface heat and freshwater fluxes are necessary for setting up the flow.

Sandstrom (1908, 1916) postulated a theorem that in order to maintain a circulation the heating source must be placed at a level below that of the cooling. Sandstrom reported upon his laboratory experiments, and stated that when the heating source was placed at a level higher than that of the cooling, no circulation was observed. The Sandstrom theorem has remained a point of debate for the past century. An intricate case is what may happen if the heating and cooling sources are placed on the same level? (Such a setting is now referred to as horizontally differential heating.) Rossby (1965) carried out laboratory experiments in which a tank filled with fluid was horizontally differentially heated from the bottom. He observed that such heating/cooling does drive a circulation that penetrates to the whole depth of the tank, which he claimed is in contradiction with the Sandstrom theorem. Recently, Paparella and Young (2002) proposed a theorem for horizontal convection; however, their discussion was focused on the case of a Boussinesq fluid and with a constant thermal expansion coefficient.

Although common wisdom is that heating/cooling from above or below is analogous/symmetric, this may not be true. In fact, in this study we will show that energetics of the circulation may be quite different

Corresponding author address: Rui Xin Huang, Dept. of Physical Oceanography, Woods Hole Oceanographic Institution, Woods Hole, MA 02543.
E-mail: rhuang@whoi.edu

from heating/cooling from above or below, although the circulation patterns may look rather similar under the assumption of a uniform vertical mixing coefficient.

This study is focused on a simple model ocean with thermal forcing only. Our main goal is to understand the gravitational potential energy (GPE) balance for the meridional overturning circulation in the ocean. We will show that the essential ingredient for the Rossby experiments is GPE generated by heating from below to a fluid that has a thermal expansion coefficient, which increases with temperature. When an infinitely thin water parcel near the bottom is heated, thermal expansion of this parcel pushes the whole water column above upward. In this process, the internal energy is converted to GPE. (Conceptually, this process involves expansion of the water parcel, so internal energy is first converted to kinetic energy, and then GPE). The amount of GPE for a water column with unit horizontal area, located from the sea surface to a depth of *h,* is

$$\chi_0 = mgh_{\text{cen}},$$

where g is gravity, h_{cen} is the center of mass related to the reference level for GPE, and $m = \int_{-h}^{0} \rho_0(z)\, dz$ is the total mass of the water column, where $\rho_0(z)$ is the density profile in the water column. Assuming a water parcel at depth h and with an initial thickness of Δh receives an amount of heat Q, this parcel expands after heating to a new thickness of $\Delta h + \delta h$, $\delta h \simeq (\alpha Q/\bar{\rho} c_p)$, where α is the thermal expansion coefficient, c_p is the specific heat under constant pressure, and $\bar{\rho}$ is the reference density. Thus, after heating, the whole water column above is pushed upward for a distance of δh, and the total GPE of this water column is

$$\chi_1 = mg(h_{\text{cen}} + \delta h).$$

The net change in GPE for the water column after heating a water parcel is

$$\Delta\chi = \frac{g\alpha Q}{c_p} \frac{\int_{-h}^{0} \rho_0(z)\, dz}{\bar{\rho}} \simeq \frac{g\alpha h Q}{c_p}. \tag{1}$$

Note that the thickness Δh of the water parcel is assumed to be much smaller than h, so changes in GPE of this water parcel are neglected in this analysis. In addition, water density is nearly constant, so that $\int_{-h}^{0} \rho_0(z)\, dz \simeq \bar{\rho} h$.

From this formula, it is clear that in order to make heating an efficient source of energy, it should be placed at deep levels. Geothermal heating is such an example. On the contrary, heating at the surface will not generate much mechanical energy, if the depth of the heat penetration is very shallow.

In the discussion above we assume the water parcel is at a depth of *h.* If the water parcel is at the sea surface, the GPE increase is due to the upward motion of the center of mass, $\delta h/2$. Thus, the corresponding formula is $\Delta\chi \simeq (g\alpha h Q/ac_p)$, where $a = 2$ if heat applies to the sea surface and $a = 1$ if heat applies to the seafloor.

Note that for a steady state, the total amount of heat through heating and cooling should be balanced. Assuming specific heat is constant, the GPE generated from thermal forcing should be

$$\Delta\chi = \frac{gQ}{ac_p}(\alpha_h h_h - \alpha_c h_c), \tag{2}$$

where α_h (α_c) and h_h (h_c) are the thermal expansion coefficient and geometric height for the heating (cooling) source, respectively. Thus, when heating and cooling take place at the same level, their effect will be canceled for the most part, if the thermal expansion coefficient is constant. However, the thermal expansion coefficient of water increases with temperature, because an equilibrium state GPE source generated by heating at the bottom is much larger than a GPE sink generated by cooling at the bottom. Thus, there is a large amount of net GPE generated, which can be used to sustain the circulation. From Eq. (2), in order to generate a large amount of GPE, heating/cooling sources should be placed at a great depth. Obviously, surface thermal forcing cannot generate much GPE at all because the penetration depth of the thermal forcing is quite small, on the order of a few meters in the ocean.

The discussion above is based on the assumption of a specified depth of heating and cooling. However, the stability of heating/cooling should be included as well. During surface heating, the water column remains stable; however, cooling creates dense water at the top of the water column, which induces a convective adjustment. During the convective adjustment, the center of mass moves downward. Thus, the effective geometric height of surface cooling is not at the surface; instead, it is at half the depth of the mixed layer. As a result, surface heating/cooling work together as a sink of GPE. This is an important extension of the Sandstrom theorem, and this is one of the main focuses of this study.

To simplify the problem, here we will study the thermal circulation only, and this paper is organized as following. The model formulation is discussed in section 2, and the circulation patterns are discussed in section 3. The core of this paper is the detailed analysis of the GPE balance for the four numerical experiments in section 4, and we draw conclusions in section 5.

2. Model formulation

Many traditional oceanic circulation models are based on Boussinesq approximations, so there are artificial sources and sinks in such models (Huang 1998). Furthermore, due to the replacement of mass conservation with volume conservation, GPE is not conserved in such models, so diagnosing the GPE balance is very difficult, if not impossible. To avoid these problems, this study is based on a mass-conserving oceanic general circulation model, PCOM, developed by Huang et al. (2001).

The numerical model used in this study is a pressure-η coordinate model, a slight modification from the pressure-σ coordinate model of Huang et al. (2001). The η coordinates are defined as $\eta = (p - p_t)/r_p$, $r_p = (p_b - p_t)/p_B$, where p_b is the bottom pressure, p_t is the sea level atmospheric pressure, and $p_B = p_B(x, y)$ is the time-invariant reference bottom pressure. In this study, we will set $p_t = 0$ and p_B equal to the bottom pressure p_b of the initial state of rest.

The model ocean is a 60° × 60° basin 5 km deep. The southern (northern) boundary of the model ocean is the equator (60°N). The horizontal resolution is 2° × 2°, and there are 30 layers stretched from a thin layer of 30 m at the top boundary layer to about 300 m at the bottom. (The actual layer thickness is in pressure units. Since the model starts from an initial state of rest and with a uniform temperature of 10°C, a 30-m layer corresponds to a pressure increment of 30.8 dbar. The layer thickness slightly evolves with time because the model has pressure-η coordinates. However, most of our results will be presented in terms of geometric height.)

The equation of state has two versions.

1) In the case of a linear equation of state,

$$\rho = \rho_0(1 - \alpha T), \tag{3a}$$

where $\alpha = 0.000\,152\,3\ ^\circ\mathrm{C}^{-1}$ is a constant thermal expansion coefficient.

2) For the case of a nonlinear equation of state, we use a cubic polynomial expression for the temperature dependency:

$$\rho = 1028.106 + 0.7948(S - 35.0) - 0.059\,68T - 0.0063T^2 + 3.7315 \times 10^{-5}T^3. \tag{3b}$$

With $S = 35$, this equation gives a density rather close to that of seawater.

The model is subject to the thermal relaxation boundary condition for the surface temperature; with a reference temperature of 0°C that linearly increases to 25°C in the meridional direction. There is no wind stress or haline forcing for this study.

For all cases, a constant vertical mixing rate of $0.3 \times 10^{-4}\ \mathrm{m^2\ s^{-1}}$ and a horizontal mixing rate of $10^3\ \mathrm{m^2\ s^{-1}}$ is used. A bottom friction parameterization is included (Cox 1989), and a nondimensional bottom friction parameter is chosen at $c_0 = 2.6 \times 10^{-3}$. Although most current low-resolution model simulations are based on the rotation of a mixing tensor and an eddy parameterization, these numerical schemes make the GPE diagnosis more complicated. To highlight the essential physics of the GPE balance in the model ocean, no mixing tensor rotation or eddy transport is used in this study. The time step is 1 day for temperature and 1.2 h for velocity.

3. Structure of the circulation

Four cases have been examined in detail in this study: case A, surface heating at low latitudes and cooling at a high latitude, with a linear equation of state; case B, same as in case A but with a nonlinear equation of state; case C, bottom heating at high latitudes and cooling at low latitudes, with a linear equation of state; and case D, same as in case C but with a nonlinear equation of state.

The rationale for placing the heating at high latitudes for cases C and D is as follows. If the model ocean was heated along the equator from below, strong convection would develop there. Since the Coriolis parameter is zero along the equator, the structure of the circulation for such cases would be quite different from that associated with convection developed at high latitudes, such as in cases A and B. As will be shown shortly, by placing the heating at a high-latitude seafloor, the circulation patterns are near mirror images of the cases of heating from the surface along the equator.

We also flip the vertical layer thickness arrangement, so that the vertical resolution is fine near the bottom in order to resolve the strong stratification associated with the thin cold-bottomed boundary layer for cases C and D.

In each case the model is run for 10 000 yr to reach a steady state. The structures of the circulation in all these cases look rather similar when compared with each other, so there is no need to show all of them. As examples, we include the temperature distribution along a meridional section through the middle of the basin (top panel in Fig. 1). It is clear that the temperature distribution in cases A and C is a nearly perfect mirror image. Similarly, the meridional streamfunction from these two cases is also a mirror image of each other (bottom panel in Fig. 1).

To extract the essential difference between cases A and C, we define the difference in temperature and

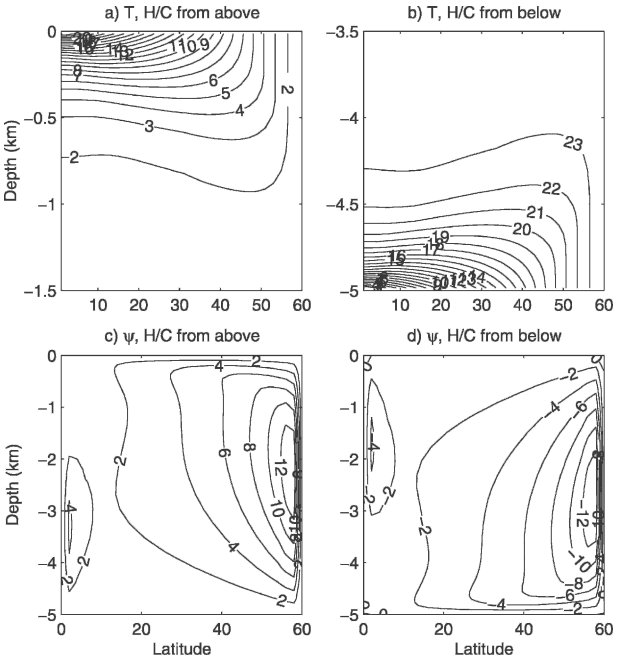

FIG. 1. Temperature and meridional overturning streamfunction (in Sv) for cases A and C.

streamfunction as $T_c - T_a = [25 - \text{flip}(T_c)] - T_a$, and $\Psi_c - \Psi_a = \text{flip}(-\Psi_c) - \Psi_a$, where flip indicates flipping the field upside down.

The differences in the structure of the circulation, such as the temperature distribution and the meridional streamfunction, are quite small (Table 1). In fact, the difference is so small that if two solutions are placed side by side, upon simple visual inspection the differences are barely noticeable (Fig. 2).

Another very interesting phenomenon is that the sea surface height (SSH) and bottom pressure perturbation (BPP) for cases A and C are exactly reversed (Fig. 3). In our model there is no bottom friction on the barotropic flow, so the flows at the surface and at the bottom are driven by the pressure gradient. These two cases are nearly antisymmetric with the vertical axis, with the exception of GPE produced by thermal forcing at the upper/lower boundary, which will be explained in Fig. 4. Thus, almost everything associated with the structure of the circulation has some kind of mirror image for these two cases.

4. Analysis of the GPE balance

In this mass coordinate, GPE is defined as $\chi = (1/g)\iiint \phi r_p \, d\eta \, dx \, dy$, where the geopotential is a diagnostic variable $\phi = gz_b + r_p \int_\eta^{p_B} (d\eta/\rho)$. The balance of the GPE in the numerical model can be diagnosed from the numerical program. Note that, in the numerical model, density $\rho = \rho(\theta, S, p)$ is a diagnostic variable, $S \equiv 35$ is set for the present study, and potential temperature is a diagnostic variable that obeys

$$\frac{\partial \theta}{\partial t} + \mathbf{u} \cdot \nabla \theta = \frac{1}{r_p}\left[\nabla_\eta \cdot (r_p \kappa_h \nabla \theta) + \frac{\partial}{\partial \eta}\left(\frac{\rho^2 g^2}{r_p} \kappa_v \frac{\partial \theta}{\partial \eta}\right) + \text{CA}\right], \tag{4}$$

where ∇_η is a two-dimensional horizontal divergent operation in pressure-η coordinates; κ_h and κ_v are the horizontal and vertical mixing coefficient ($\text{m}^2\,\text{s}^{-1}$), respectively; and CA is the contribution due to the convective adjustment, which cannot be written in simple analytical form. For steady circulation, the time-dependent term vanishes, so there is a five-term balance of GPE, including the advection (ADV), horizontal and vertical mixing (HM and VM), surface forcing (SF), and convective adjustment (CA):

$$\text{ADV} + \text{HM} + \text{VM} + \text{SF} + \text{CA} = 0. \tag{5}$$

The contribution from each term can be calculated as follows. Within one time step, changes in potential temperature in each grid box can be calculated; the corresponding density changes can be computed from the equation of state, and then changes in geopotential and GPE can be calculated afterward. Similarly, the contribution from other processes can be calculated. Note that most of these terms cannot be expressed in simple analytical forms. However, it is rather straightforward to diagnose these terms from the numerical model.

The advantage of using the pressure-η coordinates is that when the system reaches an equilibrium state, the bottom pressure does not change with time. Since thermal diffusion cannot change the total mass in each water column, at each time step the GPE sources–sinks due to changes in density associated with advection, horizontal and vertical mixing, surface forcing, and the convective adjustment can be calculated by keeping

TABLE 1. Difference in temperature (°C) and meridional streamfunction (Sv) for four cases. Note that the surface temperature range is 0°–25°C, and the meridional streamfunction maximum is approximately 13 Sv.

	$T_b - T_a$	$T_c - T_a$	$T_d - T_c$	$\Psi_b - \Psi_a$	$\Psi_c - \Psi_a$	$\Psi_d - \Psi_c$
Max	0.57	0.20	1.33	0.26	0.10	0.16
Min	−0.30	−0.30	−0.07	−3.81	−0.20	−4.98

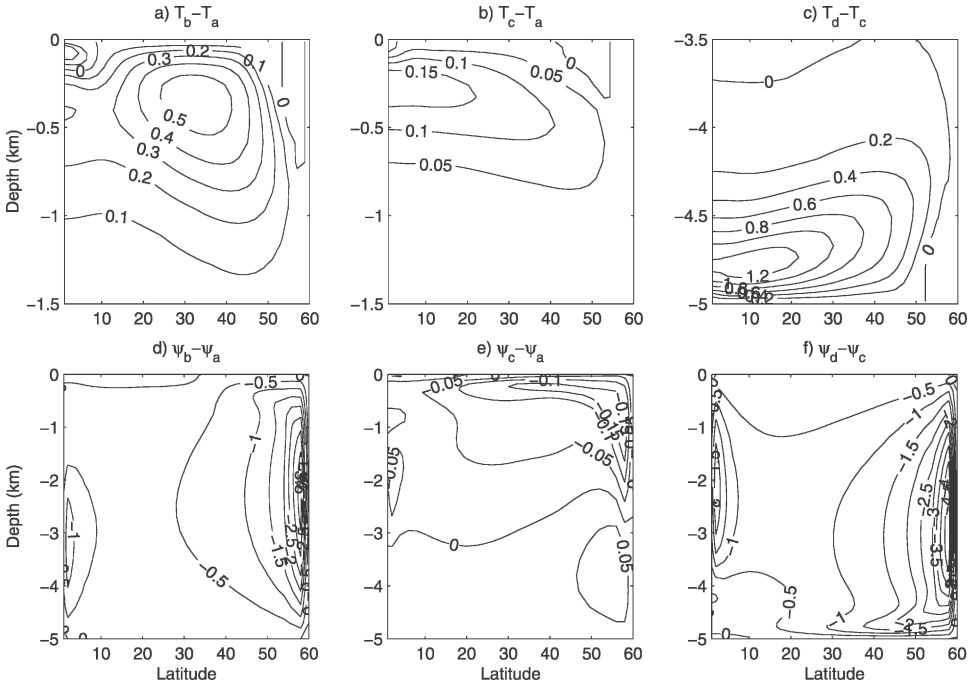

FIG. 2. Difference in temperature and meridional streamfunction (Sv) for the four cases.

track of the changes in the geopotential for each grid cell.

a. GPE balance for case A

For case A, which is forced from above and with a linear equation of state, the primary GPE balance is between the source due to vertical mixing (19.8 GW) and the loss due to the convective adjustment (17.1 GW); see Fig. 4a. There is a small portion of GPE that is converted to kinetic energy. Since the model is subject to thermal forcing only, without wind stress forcing, the conversion from GPE to kinetic energy is the only source maintaining the circulation against friction.

There is a tiny source of GPE due to the surface thermal forcing. The smallness of this source term is due to the fact that heating and cooling are exactly

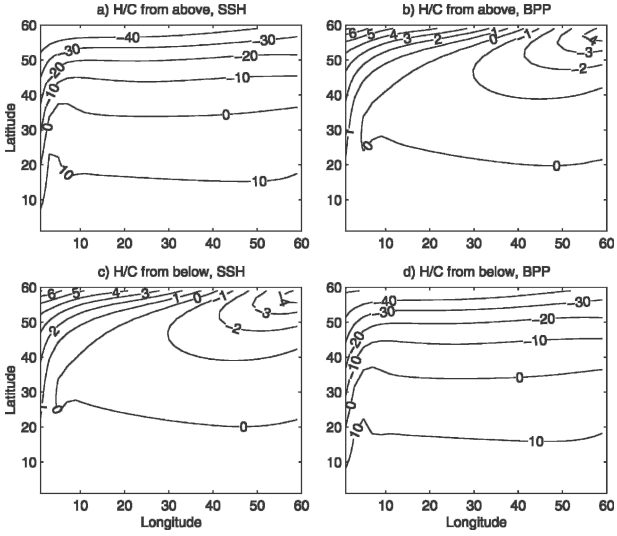

FIG. 3. SSH and BPP for cases A and C (cm).

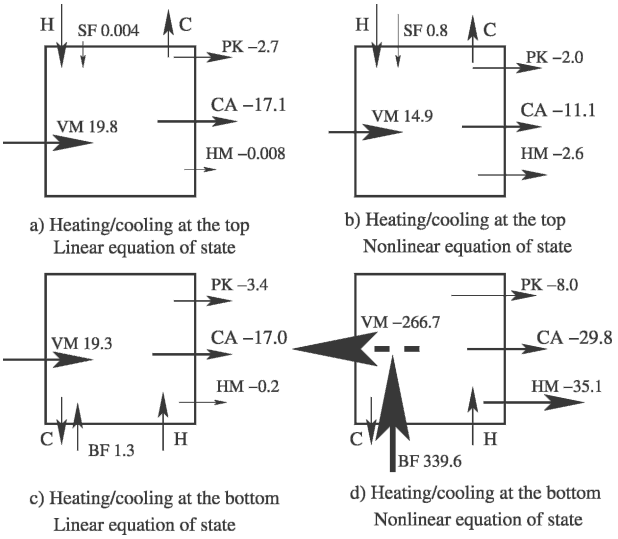

FIG. 4. GPE balance (GW): CA is the GPE sink due to convective adjustment, VM is the GPE source due to vertical mixing, PK is the sink due to the conversion from potential energy to kinetic energy, SF is the source of GPE due to surface thermal forcing, and BF is the source of GPE due to bottom thermal forcing.

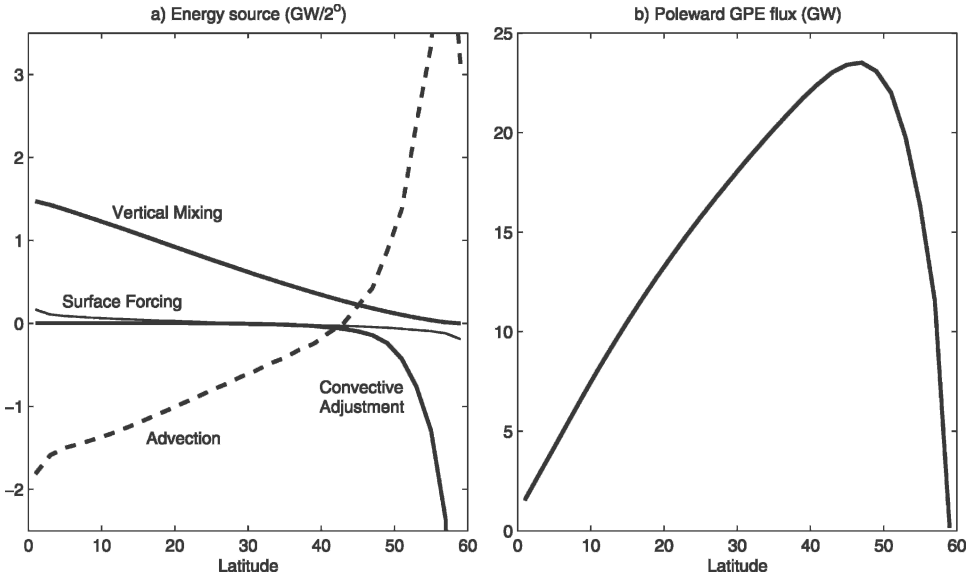

FIG. 5. GPE source–sink and balance for case A: (a) meridional distribution of GPE sources due to vertical mixing, surface forcing, advection, and convective adjustment, and (b) poleward transport of GPE.

balanced for a steady state, so the contribution to GPE is nearly canceled. If the surface layer thickness were further reduced, this term would diminish further. Since, for the most part, solar radiation can penetrate to a depth of less than 10 m, the source of GPE due to surface heating/cooling is a negligible contribution to the world oceans. (A rough estimate of GPE generated by solar radiation penetration in the world oceans is on the order of 10^{10} W.) Furthermore, convective adjustment leads to a great loss of GPE and this is the most important term in the balance of GPE for the present situation.

Note that the horizontal mixing appears as a tiny sink of GPE. Since the equation of state is linear, there is no cabbeling. However, horizontal mixing of temperature may affect the geopotential height of water columns and, thus, change the total amount of GPE for the model ocean.

These terms are nonuniformly distributed in the meridional direction (Fig. 5). The primary source of GPE is due to vertical mixing at low latitudes and the primary sink of GPE is convective adjustment, mostly confined to high latitudes (Huang and Wang 2003). Surface thermal forcing produces a small amount of GPE at low latitudes; however, this production of GPE is offset by the GPE loss due to cooling at high latitudes (Fig. 5a).

At each grid box GPE is balanced in a steady state. At lower latitudes, the primary balance of GPE is between the source due to vertical mixing and the sink due to the divergence of the advective transport of GPE. At high latitudes, GPE is primarily balanced by the transport convergence and sink due to the convective adjustment. Since this model has no wind stress forcing, energy required for sustaining the circulation against friction must come from the conversion from GPE to KE. In a steady state, the conversion from GPE to kinetic energy is $\iiint_V g\rho' w' \, dx \, dy \, dz$, where ρ' and w' are the density and vertical velocity deviations from the horizontal mean. The density deviation is negative in the southern basin, but it is positive near the northern boundary where the mean vertical velocity is negative. Thus, this conversion term is negative near the southern and northern boundaries; however, it is positive at middle latitudes, indicating that kinetic energy is converted back to GPE.

Since the convective adjustment is a large sink of GPE, the balance of GPE requires a large amount of poleward transport of GPE in the model ocean (Fig. 5b). Therefore, the balance of GPE in this model ocean as follows. GPE is generation at low latitudes primarily by vertical mixing and carried by the meridional overturning circulation to high latitudes where it is used to support the convective adjustment and conversion to kinetic energy.

In a time-dependent problem, GPE varies with time; however, changes in GPE are balanced by sources/sinks for each instance. (Because of numerical schemes, such as the leapfrog scheme, used in the model, GPE is not exactly conserved in the model for a time-dependent problem. However, these errors are small, and the bal-

ance of GPE can be diagnosed to illustrate the physical processes involved.)

As an example, we studied the annual cycle of GPE fluxes for the same model, but we subjected them to a relaxation temperature that has a simple sinusoidal cycle:

$$T^* = 25\left(1 - \frac{\theta}{\theta_N}\right) + 5\frac{\theta}{\theta_N}(1 - \sin 2\pi t), \qquad (6)$$

where $\theta_N = 60°$. In this case, the convective adjustment is active for the winter only (Fig. 6). Similarly, the surface forcing is now a sink of GPE during the cooling season, but it is a source of GPE during the heating season. On the other hand, sources of GPE due to vertical mixing and the sink of GPE due to conversion to kinetic energy remain nearly constant year round. As a result, GPE has a pronounced seasonal cycle, as is shown by the dotted line in Fig. 6. During the spring, summer, and fall seasons, GPE is accumulated primarily through vertical mixing and with a minor contribution from the surface heating. This accumulated GPE is quickly lost to convective adjustment during the winter season. This seasonal cycle reinforces the idea that cooling on the surface does not create mechanical energy—it can transfer GPE to kinetic energy only.

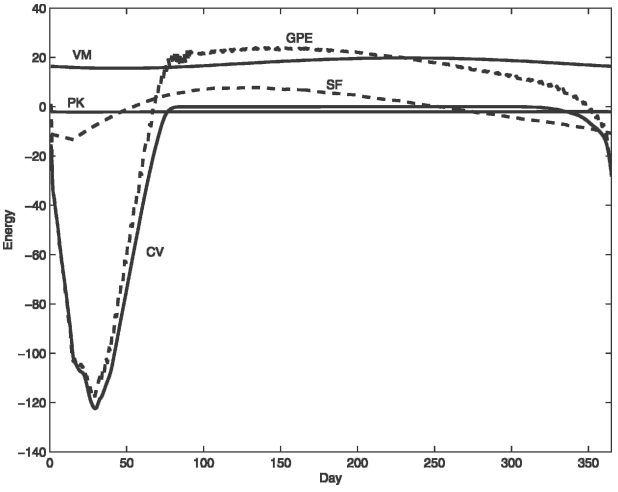

FIG. 6. Annual cycle of energy fluxes (GW): CV is the GPE sink due to convective adjustment, VM is the GPE source due to vertical mixing, PK is the sink due to the conversion from potential energy to kinetic energy, SF is the source of GPE due to surface thermal forcing, and GPE is the total amount of gravitational potential energy for the model basin.

b. GPE balance for case B

Case B is for a nonlinear equation of state, but the balance of GPE is rather similar to that in case A. Again the main balance is between the source due to vertical mixing (14.9 GW) and the sink due to the convective adjustment (11.1 GW); see Fig. 4b.

The thermal expansion coefficient of water increases with temperature, and this can cause the cabbeling phenomenon, which plays an important role in the deep-water formation in the world oceans. Cabbeling is due to the fact that the mixing of two water masses can produce water with a higher density. Because of the increases in density, the volume of the water parcels is reduced. As a result, the whole water column above moves down and GPE is reduced. Dense water masses formed through cabbeling eventually sink to a greater depth, and this has been identified as an important process involved in deep/bottom water formation in the world oceans (e.g., Foster 1972; Foster and Carmack 1976).

In the present case the decline in GPE generated by vertical mixing and the GPE loss due to the convective adjustment are due to cabbeling. Because the thermal expansion coefficient increases with temperature, it takes less energy to maintain the same temperature stratification. Similarly, the loss of GPE due to the convective adjustment is less. Overall, the energy fluxes are reduced. As a result, although the temperature distribution appears similar in these two cases (Fig. 2a), it takes much less external mechanical energy to sustain such a circulation (14.9 GW in case B, as compared with 19.8 GW in case A). In addition, the strength of the overturning circulation is reduced by about 3.8 Sv (Sv $\equiv 10^6$ m^{-3} s^{-1}; see Fig. 2d and Table 1).

Note that horizontal mixing is now a noticeable sink of GPE (-2.6 GW), and it is clearly due to cabbeling. Because the thermal expansion coefficient increases with temperature, the average density of the two water parcels after mixing is larger than the original density. As a result, the water column shrinks and leads to a release of GPE.

In addition, the source of GPE due to surface thermal forcing is slightly increased to 0.8 GW. This increase in GPE due to surface thermal forcing is due to the fact that the thermal expansion coefficient is larger at a higher temperature; thus, GPE generation due to heating overcompensates the sink due to cooling.

c. GPE balance for case C

For this case the circulation is maintained by GPE produced primarily by vertical mixing as in the previous cases. At the same time the bottom thermal forcing makes a small contribution. Note that although α is constant, the bottom pressure is not uniform. In fact a slightly larger bottom pressure on the heated end of the lower boundary surface may be the reason for a positive source of GPE.

A small, but important, difference between cases A and C is the following (Figs. 4a and 4c). As the thickness of the top layers in case A shrinks, the GPE source due to surface heating/cooling would diminish. (Note that assuming a different top layer thickness is equivalent to assuming a different degree of solar heating penetration, thus implying a different amount of GPE source due to surface forcing. This resolution dependence of the GPE source due to surface thermal forcing is an artifact of the numerical model.) On the other hand, the GPE source due to bottom heating/cooling should remain finite, regardless of how thin the bottom layer can become. This is due to the fact that the GPE source produced by bottom heating/cooling is determined by the bottom pressure, which is insensitive to the vertical resolution of the model.

Other than this minor difference in the GPE source due to surface thermal forcing, the circulation in case C is a mirror image of case A. It is a nearly perfect flip-over between these two cases. However, mirror image symmetry exists in the case of a linear equation of state only. Note that the rate of conversion to kinetic energy is slightly increased from 2.7 GW for case A to 3.4 GW for case C. This increase is due to the difference in the circulation. In particular, a fast current exists in the bottom boundary layer in case C, and it takes more energy to maintain. On the other hand, the bottom current in case A is very slow and does not dissipate much energy.

d. GPE balance for case D

Although the circulation patterns of cases C and D are rather similar, including the heat flux through the seafloor, the energetics of the model are totally different in these two cases (Figs. 4c and 4d). There is a huge amount of GPE generated by thermal forcing from below in case D (340 GW). The essential point is that the thermal expansion coefficient increases with temperature for case D, but it is constant for case C. As a result, the amount of GPE generated along the western boundary at high latitudes in case D is about twice as much as that in case C because of the difference in the thermal expansion coefficient. On the contrary, the GPE sink along the southern boundary of the basin in case D is smaller than that in case C (Fig. 7). The contributions from heating and cooling for these two cases are listed in Table 2. It is interesting to note that although the contribution from cooling is about the same in both cases, the source of GPE in case D is about twice that in case C, and this is what causes an essential difference in these two cases.

Note that in case D vertical mixing occurs because of a sink of GPE as shown in the appendix, where the following criterion is satisfied:

$$\frac{h}{\alpha}\frac{d\alpha}{dz} > 1, \quad \text{or} \quad -\frac{p}{\alpha}\frac{d\alpha}{dp} > 1. \tag{7}$$

The whole water column above moves downward after vertical mixing, so the total GPE of the water column is reduced after vertical mixing. In the present case, there is a very thin cold bottom boundary layer. The strong vertical temperature gradient within this boundary layer satisfies the instability criterion; thus, the vertical mixing above the bottom boundary layer induces a strong release of GPE. The cabbeling index is of the order of 1–200 for the bottom 200 m in the model ocean (Fig. 8); thus, vertical mixing is self-energized.

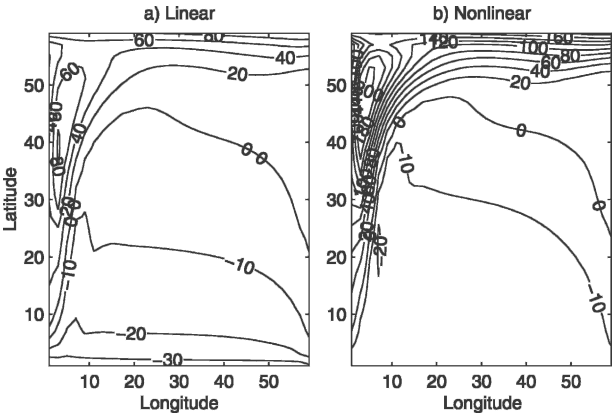

FIG. 7. GPE source and sink due to bottom thermal forcing (mW m^{-2}).

5. Discussion

We have studied the thermal circulation in a simple model ocean. Although the pattern of circulation for all of these cases is rather similar, the energetics of the circulation can be dramatically different, depending upon the equation of state used in the model and the location of the thermal forcing. In particular, the energetics of the circulation in case D (differential heating from below, plus a nonlinear equation of state) is totally different from that in cases A, B, and C.

For cases A, B, and C, the circulation depends on GPE generated by vertical mixing. Case B is an idealized version of the thermal circulation in the North Atlantic. In all three cases, if there was no external source of mechanical energy to support vertical mixing, there would be no energy supporting the motion against friction; thus, there would be no circulation, except for an extremely weak circulation driven by molecular mixing.

TABLE 2. GPE source–sink due to heating/cooling from below (GW).

	Heating	Cooling	Net
Linear	312.0	−310.7	1.3
Nonlinear	641.5	−301.9	339.6

Many numerical experiments have been carried out based on Boussinesq approximations with a constant thermal expansion coefficient and specified Rayleigh and Prandtl numbers (e.g., Rossby 1965, 1998; Paparella and Young 2002). A recent study by Wang and Huang (2005) has confirmed that a relatively slow but steady (with weakly turbulence-like time-dependent perturbations) partial penetrating circulation does exist for the cases of horizontal differential heating from the upper (or lower) boundary of a double-wall box container filled with salty water and with dimensions of $20 \times 15 \times 2.5$ cm. Thus, the so-called Sandstrom theorem is inaccurate. Recently, more rigorous theorems for horizontal convection have been proposed (e.g., Paparella and Young 2002; Siggers et al. 2004). However, these studies are based on the assumption of a constant thermal expansion coefficient. In the case of seawater, the thermal expansion coefficient is a strong nonlinear function of temperature, and the energetics of the horizontal convection for the case with nonconstant thermal expansion coefficient may be different. This is left for further study.

The energetics for case D is dramatically different from all of the other cases because GPE generated by bottom thermal forcing is the energy source of the circulation. Since vertical mixing and cabbeling is self-energized in this case, turbulence and internal waves would be sustained by cabbeling that is in turn supported by boundary thermal forcing, and there is no need for an external mechanical energy source. Note that in case D the vertical mixing rate and the temperature relaxation time are specified a priori. If the corresponding experiment is carried out in a real fluid in a laboratory, both parameters will be set by the turbulent and internal waves in the circulation system itself. Depending on how strong the turbulent motion is, mixing across the bottom boundary will set the rate of heat flux through the bottom and mixing in the interior will set the rate of energy release from cabbeling. Thus, we speculate that the system will adjust itself into a circulation in which the energetics is self-consistent. In such a circulation, the vertical (diapycnal) mixing rate is unlikely to be vertically uniform; however, at this time it seems unclear how strong the circulation will be if these laboratory experiments are carried out. Because of the tremendous dimensions of the oceans, such laboratory experiments are unrealistic. It is speculated that such circulation may be studied, using numerical models of turbulence and internal waves; however, such a challenging task is left for further study.

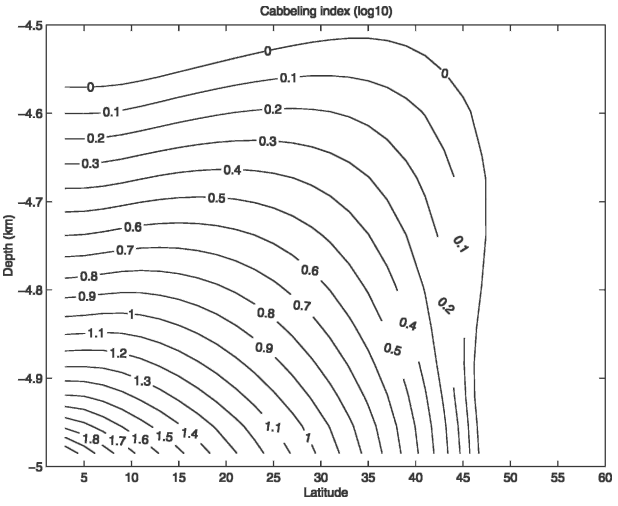

FIG. 8. Distribution of the cabbeling index for case D for a vertical section through the middle of the basin.

Although the thermal expansion coefficient normally increases with temperature for most fluids, there are counterexamples. In fact, the thermal expansion coefficient of many fluids, such as hydrogen peroxide, declines with temperature (Washburn 1928). Another counterexample is mercury: for temperature ranges below 100°C, the thermal expansion coefficient actually declines with temperature. We speculate that if such fluids were used in experiments like those of Rossby, there would be virtually no observable circulation. It is also speculated that if a fluid with a constant thermal expansion coefficient were used in the same experiment, without external mechanical energy supporting mixing there would be no observable circulation.

Acknowledgments. RXH and XZJ were supported by the National Science Foundation through Grant OCE0094807 to the Woods Hole Oceanographic Institution and the Van Alan Clark Chair of the Woods Hole Oceanographic Institution.

APPENDIX

Instability due to Cabbeling

Assume that two boxes, with box 1 on top of box 2, of water are located at the depth of h, with equal thickness Δh (Fig. A1). Assuming the thermal energy (over a time interval of δt and per unit of horizontal area) associated with vertical mixing is $(\kappa \rho_0 c_p/\Delta h)(T_1 -$

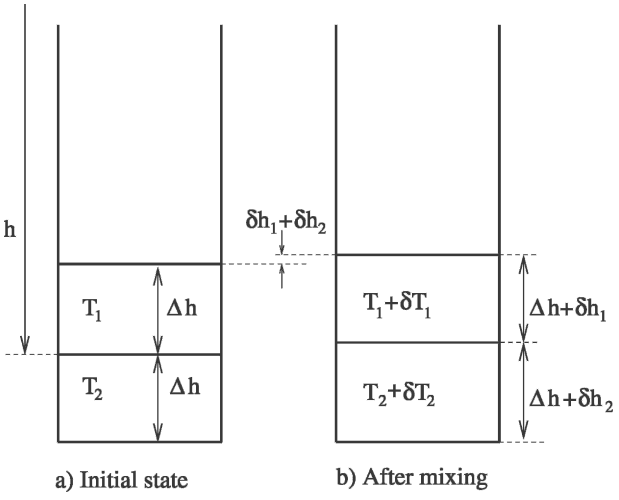

FIG. A1. Sketch of a water column under vertical thermal mixing.

$T_2)\delta t$, where κ is the vertical mixing coefficient, ρ_0 is the mean reference density, and c_p is the specific heat under constant pressure, which is an assumed constant, then, the lower box is warmed up; that is, $\delta T_2 = (\kappa\rho_0/\Delta h^2\rho_2)(T_1 - T_2)\delta t = (\kappa/\Delta h^2)(T_1 - T_2)\delta t + o(\varepsilon) > 0$. Here, $\varepsilon = 1 - \rho_0/\rho_2 \ll 1$ is a small parameter, so $o(\varepsilon)$ is the high-order term that is negligible for our analysis below. Similarly, we have $\delta T_1 = -(\kappa\rho_0/\Delta h^2\rho_1)(T_1 - T_2)\delta t = -(\kappa/\Delta h^2)(T_1 - T_2)\delta t + o(\varepsilon) < 0$. Thus, to a good approximation, $\delta T_1 \approx -\delta T_2 < 0$. The center of mass of box 2 is displaced upward for a distance of $\delta h_2/2$, and the center of mass of box 1 is moved upward for a distance of $\delta h_2 + \delta h_1/2$, while the center of mass for the water column above these two boxes moves a distance of $\delta h_2 + \delta h_1$. Changes in GPE for box 1, box 2, and the water column above are

$$\delta\chi_1 = 0.5\rho g\Delta h^2(2\alpha_2 - \alpha_1)\delta T_2, \tag{A1}$$

$$\delta\chi_2 = 0.5\rho g\Delta h^2\alpha_2\delta T_2, \quad \text{and} \tag{A2}$$

$$\delta\chi_h = \rho g\Delta h(\alpha_2 - \alpha_1)\delta T_2. \tag{A3}$$

The net change in GPE for the whole column is

$$\delta\chi = \rho g\Delta h[-h(\alpha_2 - \alpha_1) + \Delta h\overline{\alpha}]\delta T_2, \tag{A4}$$

where $\overline{\alpha} = 0.5(\alpha_1 + \alpha_2)$. For small δh, this is reduced to

$$\delta\chi = -\kappa\rho g\Delta T\alpha\left(\frac{h}{\alpha}\frac{d\alpha}{dz} - 1\right). \tag{A5}$$

Note that the second term on the right-hand side of (A1) is always positive and that means vertical mixing requires an external source of mechanical energy. On the other hand, the first term on the right-hand side of (A5) is negative definite because of a stable temperature stratification, $\alpha_1 > \alpha_2$. That means cabbeling tends to reduce the amount of GPE required to support vertical mixing. If the vertical cabbeling index satisfies

$$\frac{h}{\alpha}\frac{d\alpha}{dz} > 1, \quad \text{or} \quad -\frac{p}{\alpha}\frac{d\alpha}{dp} > 1, \tag{A6}$$

then the total change of GPE is negative after vertical mixing; that is, vertical mixing can release GPE and is thus self-energized. It is clear that the favorite site is a strong vertical gradient at great depths.

REFERENCES

Cox, M., 1989: An idealized model of the World Ocean. Part I: The global-scale water masses. *J. Phys. Oceanogr.,* **19,** 1730–1752.

Foster, T. D., 1972: An analysis of the cabbeling instability in sea water. *J. Phys. Oceanogr.,* **2,** 294–301.

——, and E. C. Carmack, 1976: Frontal zone mixing and Antarctic bottom water formation in the southern Weddell Sea. *Deep-Sea Res. Oceanogr. Abstr.,* **23,** 301–317.

Huang, R. X., 1998: On available potential energy in a Boussinesq ocean. *J. Phys. Oceanogr.,* **28,** 669–678.

——, 1999: Mixing and energetics of the thermohaline circulation. *J. Phys. Oceanogr.,* **29,** 727–746.

——, 2004: Ocean, energy flow. *Encyclopedia of Energy,* C. J. Cleveland, Ed., Vol. 2, Elsevier, 497–509.

——, and W. Wang, 2003: Gravitational potential energy sinks in the oceans. *Near-Boundary Processes and Their Parameterization: Proc. 'Aha Huliko'a Hawaiian Winter Workshop,* Honolulu, HI, University of Hawaii at Manoa, 239–247.

——, X.-Z. Jin, and X.-H. Zhang, 2001: An oceanic general circulation model in pressure coordinates. *Adv. Atmos. Sci.,* **18,** 1–22.

Munk, W. H., and C. Wunsch, 1998: The moon and mixing: Abyssal recipes II. *Deep-Sea Res. I,* **45,** 1977–2010.

Paparella, F., and W. R. Young, 2002: Horizontal convection is non-turbulent. *J. Fluid Mech.,* **205,** 466–474.

Rossby, T., 1965: On thermal convection driven by non-uniform heating from below; an experimental study. *Deep-Sea Res. Oceanogr. Abstr.,* **12,** 9–16.

——, 1998: Numerical experiments with a fluid heated non-uniformly from below. *Tellus,* **50A,** 242–257.

Sandstrom, J. W., 1908: Dynamicsche Versuche mit Meerwasser. *Ann. Hydrogr. Mart. Meteor.,* **36,** 6–23.

——, 1916: Meteorologische Studien im schwedischen Hochgebirge. *Goteborgs K. Vetenskaps-och Vitterhetssamhalles Handl.,* Ser. 4, Vol. 22, No. 2, 48 pp.

Siggers, J. H., R. R. Kerswell, and N. J. Balmforth, 2004: Bounds on horizontal convection. *J. Fluid Mech.,* **517,** 55–70.

Wang, W., and R. X. Huang, 2005: An experimental study on thermal circulation driven by horizontal differential heating. *J. Fluid Mech.,* **540,** 49–73.

Washburn, E. W., Ed., 1928: *International Critical Tables of Numerical Data, Physical, Chemistry and Technology*. McGraw-Hill, 444 pp.

Wunsch, C., 2002: What is the thermohaline circulation? *Science,* **298,** 1179–1181.

——, and R. Ferrari, 2004: Vertical mixing, energy, and the general circulation of the oceans. *Annu. Rev. Fluid Mech.,* **36,** 281–314.